ELSEVIER

Chemical Engineering Journal 131 (2007) 233–244

Chemical Engineering Journal

www.elsevier.com/locate/cej

Thermodynamic modeling and analysis of biomass gasification for hydrogen production in supercritical water

Youjun Lu, Liejin Guo *, Ximin Zhang, Qiuhui Yan

State Key Laboratory of Multiphase Flow in Power Engineering (SKLMF), Xi'an Jiaotong University, Xi'an, Shaanxi 710049, China

Received 23 February 2006; received in revised form 7 October 2006; accepted 24 November 2006

Abstract

Biomass gasification in supercritical water is a promising technology for hydrogen production by utilizing wet biomass. A new experimental system of biomass gasification in supercritical water was built in SKLMF. In this paper, a comprehensive thermodynamic analysis, including chemical equilibrium in the reactor, gas–liquid equilibrium in the high-pressure separator, exergy and energy analysis of the whole system, was conducted. Chemical equilibrium model is based on minimizing Gibbs free energy. By chemical equilibrium analysis in the reactor, rules of the main parametric effects on biomass gasification in supercritical water are obtained. Simultaneously, a high-pressure gas–liquid equilibrium model was proposed based on modified universal functional activity coefficient (UNIFAC) model, Soave–Redlich–Kwong (SRK) equation of state and modified Huron–Vidal second-order (MHV2) mixing rule. Effects of pressure, temperature and water recycled ratio on gas–liquid equilibrium in high-pressure separation were discussed. Finally, results from energy and exergy analysis show that energy and exergy efficiencies of the whole system are in excess of 40% and increase with increasing heat transfer efficiencies. Energy loss of the system is caused mainly by heat transfer and exergy loss is mainly caused by heat transfer and chemical reaction. Our research provided a thermodynamic tool for improvement of design and operation optimization of biomass gasification system in SKLMF, which may be also applicable to other biomass gasification system.

Keywords: Hydrogen production; Supercritical water; Biomass gasification; Chemical equilibrium; Phase equilibrium; Energy; Exergy

1. Introduction

Compared with fossil fuel, biomass is a clean energy with zero CO_2 emission, because CO_2 is fixed by photosynthesis during biomass growth and released again during utilization. Due to its low energy density, direct use of biomass is not convenient. Thus, it is necessary to convert biomass to fuel gas, such as hydrogen, which can be used cleanly and highly efficiently in fuel cells. Thermo-chemical gasification is likely to be the most cost-effective conversion process. However, a large portion of biomass is wet, and this causes high drying costs in classical thermo-chemical gasification process [1]. With the advantage of avoiding drying process, biomass gasification in supercritical water (SCW) is a promising technology for the utilization of wet biomass.

SCW possesses properties much different from those of liquid water. The dielectric constant of SCW is much lower, there is much less hydrogen bonds and their strength is much weaker. As a result, SCW behaves like organic solvents so that many organic compounds have very high solubility in it. Moreover, gases are miscible in SCW. Thus, chemical reaction can be conducted in a single supercritical phase reaction medium. High concentrations of reactants can often be attained and there are no interphase mass transport processes to hinder reaction rates [2]. As a result, biomass gasification in SCW has a high reaction rate. In addition, biomass gasification in SCW has high gasification efficiency at much lower temperatures of approximately 673 K compared with conventional gasification [3]. Furthermore, biomass gasification in SCW produces higher concentration of hydrogen in product gas, because the high water excess favors the formation of H_2 and CO_2 instead of CO.

So far various experimental investigations into gasification of biomass model compounds and real biomass in SCW have been carried out [1,3–16]. But the work on thermodynamic analysis of this process is limited. Thermodynamic analysis is very helpful in providing theoretical guidance for optimization of design and operation of biomass gasification system. Tang and Kitagawa [17] and Yan et al. [18] performed chemical

* Corresponding author. Tel.: +86 29 8266 3895; fax: +86 29 8266 9033.
E-mail address: lj-guo@mail.xjtu.edu.cn (L. Guo).

1385-8947/$ – see front matter © 2006 Elsevier B.V. All rights reserved.
doi:10.1016/j.cej.2006.11.016

Nomenclature

a	co-energy parameter in the SRK EOS
a_{ij}	the molar number of element i in compound j
a_{nm}, $a_{nm,1}$, $a_{nm,2}$	UNIFAC interaction parameters
b	co-volume parameter in the SRK EOS
b_i^0	the total molar number of element i in the initial reactant
C_p	specific heat capacity
C_1, C_2, C_3	Mathias–Copeman parameters
E_X, $E_{X,ph}$, $E_{X,c}$, $E_{X,Q}$	exergy, physical exergy, chemical exergy and heat exergy, respectively
f_i	fugacity of component i
g, g^E	Gibbs free energy and excess Gibbs free energy
H, H_o^*	enthalpy and enthalpy at reference state
K	equilibrium ratio
LHV	low heating value
n_j	molar number of component j
P	pressure
q_1, q_2	parameters in MHV2 mixing rule
Q_k	van der Waals surface area of group k
r_i	volume parameters of component i
R	gas constant
R_k	van der Waals volume of group k
S, S_o^*	entropy and entropy at reference state
T	temperature
V	specific volume
x_i	molar fraction of component i in the liquid phase
y_i	molar fraction of component i in the gas phase
z_i	molar fraction of component i
Z	compress factor
Z_O, Z_C, Z_H, Z_N	weight fractions of oxygen, carbon, hydrogen and nitrogen, respectively, in the biomass

Greek symbols

Φ_i	fugacity coefficient of component i
Γ_k, $\Gamma_k^{(i)}$	activity coefficient of group k and activity coefficient of group k in molecule i, respectively.
Θ_m	molar fraction of surface area of group m
$\varepsilon_{0,i}$	standard chemical exergy of a pure chemical compound i
γ_i	activity coefficient of component i
η_{en}, η_{ex}	energy and exergy efficiency, respectively
μ_i	chemical potential of component i
$\upsilon_k^{(i)}$	number of structural groups of type k in molecule i
ω	acentric factor
Ψ_{nm}	UNIFAC group interaction parameter between groups n and m

Superscripts

C	combinatorial part
g	gas phase
l	liquid phase
R	residual part
*	ideal gas

Subscript

c	critical parameter

equilibrium analysis of hydrogen production by biomass gasification in SCW based on Gibbs free energy minimization. Feng et al. [19] calculated driving forces and phase equilibrium for hydrothermal upgrading in sub-critical water and biomass gasification in SCW. Calzavara et al. [20] evaluated biomass gasification in SCW process for hydrogen production and energy efficiency of the process was calculated in the ideal case. Matsumura and Minowa [21] conducted fundamental design of SCW fluidized bed for biomass gasification and thermal efficiency for the ideal case was also calculated. Yoshida et al. [22] performed comprehensive comparison of efficiencies and CO_2 emissions between biomass energy conversion technologies and the results show that SCW gasification combined cycle for electricity generation is the most efficient for high moisture content biomass.

An experimental system was built in SKLMF to study biomass gasification in SCW for hydrogen production, and the objective of this paper is to examine the thermodynamics of biomass gasification process in SCW based on the experimental system. Thermodynamic models for chemical equilibrium in the reactor and gas–liquid equilibrium in high-pressure separator were developed, and exergy and energy analysis of the whole system were conducted. According to the thermodynamic analysis, some advice was present for improvement and operation optimization of the experimental system.

2. Experimental system for biomass gasification in SCW

Fig. 1 shows the schematic of experimental system for biomass gasification in SCW in SKLMF. The system includes mainly reactor, preheater, heater exchanger, high-pressure separator (SPE1), low-pressure separator (SPE2), and so on. Biomass feedstock at room temperature is pressurized by high-pressure pump 1, and then enters the reactor. At the same time, water with larger flow rate is compressed by the high-pressure pump 2, and then heated to high temperature in the heat exchanger and preheater. At the inlet of reactor, biomass feedstock with small flow rate and high-temperature water with larger flow rate mix together, so biomass feedstock is heated quickly to supercritical temperature. Faster heating of biomass to high temperature increases the biomass gasification efficiency according to our previous study [16]. After leaving the reactor, the high temperature fluid is cooled in the heat exchanger firstly with the heat being recycled, and is then cooled to environmental temperature in the cooler. In SPE1, product CO_2 is separated from product H_2 by high-pressure water absorption because solubility of CO_2 in high-pressure water is much larger than that of H_2. Gas phase in SPE1 is mainly composed of H_2. H_2 from SPE1 is then decompressed. CO_2 absorbed in the liquid phase in SPE1 is finally released in SPE2. When thermodynamic analysis is conducted, it is assumed that the H_2 is purified to a level suitable for a H_2/O_2

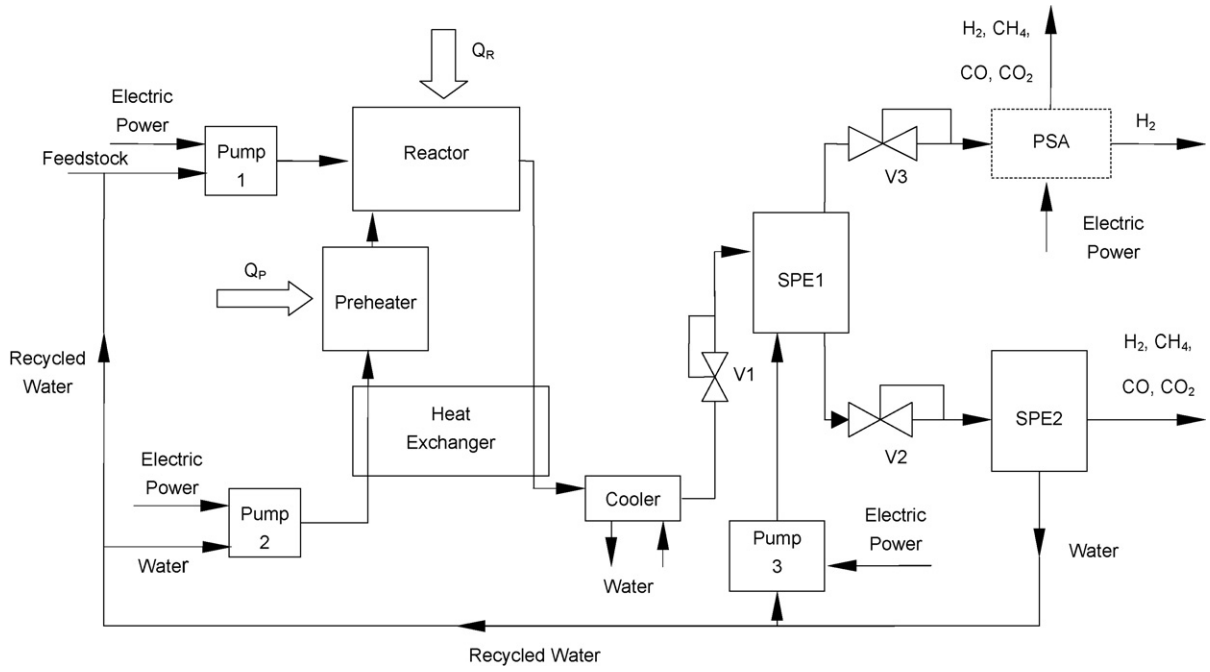

Fig. 1. Schematic of biomass gasification process for hydrogen production in SCW.

fuel cell (greater than 99.9% with CO concentration less than 5 ppm) by pressure swing absorption (PSA).

3. Thermodynamic model and method

3.1. Chemical equilibrium

Gibbs free energy of a system, with fixed T and P, can be expressed as a linear combination of chemical potential of each component in the system.

$$g = \sum_{j=1}^{n} \mu_j n_j \tag{1}$$

where n_j and μ_j are molar number and chemical potential of component j, respectively.

Equation of element conservation is described as:

$$\sum_{j=1}^{n} a_{ij} n_j - b_i^0 = 0, \quad i = 1, \ldots, l \tag{2}$$

where a_{ij} is molar number of element i in compound j, and b_i^0 is the total molar number of element i in the initial reactant.

Gibbs free energy is the minimum when a multicomponent system reaches chemical equilibrium. Minimizing Gibbs free energy of a system, with fixed T and P, is a simple constrained optimization problem. The constraints can be removed with the method of Lagrange multipliers.

Chemical potential of component i (μ_i) can be calculated by the following expression:

$$\mu_i(T, P) = \mu_i^0(T) + RT \ \ln f_i \tag{3}$$

where R is ideal gas constant, $\mu_i^0(T)$ the chemical potential of component i in standard state, and f_i is partial fugacity of component i. f_i is calculated by the equation of state proposed by DUAN [23]. More details of the model were described in our previous work [18].

3.2. Gas–liquid equilibrium

At gas–liquid equilibrium, the fugacity of component i in gas phase equals to that in liquid phase. At given temperature T and pressure P, the following equations can be obtained:

$$f_i^{\mathrm{g}} = f_i^{\mathrm{l}}, \quad i = 1, 2, \ldots, n \tag{4}$$

f_i is calculated by Soave–Redlich–Kwong (SRK) equation of state:

$$P = \frac{RT}{V - b} - \frac{a}{V(V + b)} \tag{5}$$

where parameter b for mixture is derived from linear mixing rule:

$$b = \sum_{i=1}^{c} z_i b_{ii} \tag{6}$$

in which parameter b_{ii} is for corresponding pure component

$$b_{ii} = 0.08664 \frac{RT_{ci}}{P_{ci}} \tag{7}$$

Parameter a in Eq. (5) for pure component is obtained from

$$a_{ii} = 0.4286 \frac{R^2 T_{ci}^2}{P_{ci}} [f(T_{ri})]^2 \tag{8}$$

Table 1
The C_i constants and critical parameters of pure components

Component	C_1	C_2	C_3	T_c (K)	P_c (MPa)
H_2	0.1332	0.0000	0.0000	33.2	1.297
CO	0.5836	0.0000	0.0000	132.9	3.496
CO_2	0.8653	−0.4386	1.3447	304.2	7.376
CH_4	0.5472	−0.3992	0.5751	190.6	4.600
C_2H_4	0.8479	−0.3421	0.6603	282.4	5.040
C_2H_6	0.6853	−0.4284	0.7382	305.4	4.848
H_2O	1.0873	−0.6377	0.6345	647.3	22.048

where $T_r = T/T_c$, $f(T_r)$ is given by Mathias and Copeman [24]

$$f(T_r) = \begin{cases} 1 + C_1(1 - \sqrt{T_{ri}}) + C_2(1 - \sqrt{T_{ri}})^2 + C_3(1 - \sqrt{T_{ri}})^3, & T_{ri} < 1 \\ 1 + C_1(1 - \sqrt{T_{ri}}), & T_{ri} > 1 \end{cases} \quad (9)$$

C_1, C_2 and C_3 shown in Table 1 were estimated from the pure-component vapor pressure.

Parameter a for mixture is calculated by modified Huron–Vidal second-order (MHV2) mixing rule [25],

$$q_1\left(\alpha_{\text{mix}} - \sum_{i=1}^{c} z_i\alpha_{ii}\right) + q_2\left(\alpha_{\text{mix}}^2 - \sum_{i=1}^{c} z_i\alpha_{ii}^2\right) = \frac{g^{\text{E}}}{RT} + \sum_{i=1}^{c} z_i \ln\left(\frac{b}{b_{ii}}\right) \quad (10)$$

where $\alpha_{\text{mix}} = a/bRT$, $\alpha_{ii} = a_{ii}/b_{ii}RT$, $q_1 = -0.478$, $q_2 = -0.0047$ and g^{E} is excess Gibbs energy, which is given by

$$\frac{g^{\text{E}}}{RT} = \sum_{i=1}^{c} z_i \ln\gamma_i \quad (11)$$

where γ_i is the activity coefficient of the component i, and γ_i, is obtained from the modified universal functional activity coefficient (UNIFAC) model [26]. Some groups, such as H_2, CO, CO_2, CH_4, C_2H_4, C_2H_6 and H_2O, are defined in the modified UNIFAC model.

The activity coefficient is expressed as

$$\ln\gamma_i = \ln\gamma_i^{\text{C}} + \ln\gamma_i^{\text{R}} \quad (12)$$

The first term on the right-hand side of Eq. (12) represents the combinatorial part of the activity coefficient and the second term refers the residual part.

In the modified UNIFAC model, the combinatorial part is described as

$$\ln\gamma_i^{\text{C}} = 1 - \varphi_i + \ln\varphi_i \quad (13)$$

where

$$\varphi_i = \frac{r_i^{2/3}}{\sum_j x_j r_j^{2/3}}, \quad r_i = \sum_k \upsilon_k^{(i)} R_k \quad (14)$$

In Eq. (14), R_k is van der Waals volume of group k and $\upsilon_k^{(i)}$ is the number of structural groups of type k in molecule i.

Table 2
Molecular surface area and volume values

	Gas						
	H_2	CO	CO_2	CH_4	C_2H_4	C_2H_6	H_2O
R_k	0.8320	2.0940	2.592	2.244	3.1482	3.6044	0.9200
Q_k	1.1410	2.1200	2.522	2.312	2.9700	3.392	1.4000

The residual part in Eq. (12) is represented as

$$\ln\gamma_i^{\text{R}} = \sum_k \upsilon_k^{(i)}(\ln\Gamma_k - \ln\Gamma_k^{(i)}) \quad (15)$$

Γ_k and $\Gamma_k^{(i)}$ are activity coefficient of group k and that of group k in molecule i, respectively.

$$\ln\Gamma_k = Q_k\left[1 - \ln\left(\sum_m \Theta_m\Psi_{mk}\right) - \sum_m \frac{\Theta_m\Psi_{km}}{\sum_n \Theta_n\Psi_{nm}}\right] \quad (16)$$

where

$$\Theta_m = \frac{Q_m X_m}{\sum_n Q_n X_n}, \quad X_m = \frac{\sum_j \upsilon_m^{(i)} x_j}{\sum_j \sum_n \upsilon_n^{(j)} x_j} \quad (17)$$

Q_k is van der Waals surface area of group k. Values of Q_k and R_k are shown in Table 2. Ψ_{nm} in Eq. (16) can be calculated from

$$\Psi_{nm} = \exp\left(-\frac{a_{nm}}{T}\right) \quad (18)$$

where a_{nm} is interaction parameter between groups n and m in the modified UNIFAC model. Further, values of all gas–gas interaction parameters were assigned to be zero. To describe the temperature dependence of the interaction parameters (a_{nm}), two terms were used

$$a_{nm} = a_{nm,1} + a_{nm,2}(T - T_0) \quad (19)$$

T_0 is a reference temperature (298.15 K). $a_{nm,1}$ and $a_{nm,2}$ [27] shown in Table 3 were estimated from experimental data.

The fugacity coefficient of component i is described as

$$\ln\phi_i = \ln\frac{f_i}{z_i P} = \ln\left(\frac{RT}{P(V-b)}\right) + \left(\frac{1}{V-b} - \frac{\alpha}{V+b}\right) b_{ii} - \left(\frac{\partial(n\alpha)}{\partial n_i}\right)_{T,n_j} \ln\left(\frac{V+b}{V}\right) \quad (20)$$

Table 3
Modified UNIFAC interaction parameters

n	m	$a_{nm,1}$	$a_{nm,2}$	$a_{mn,1}$	$a_{mn,2}$
H_2	H_2O	1586.0	3.924	949.9	−0.3100
CO	H_2O	1455.0	−2.906	494.0	0.1390
CO_2	H_2O	1067.0	−0.418	226.6	−0.2410
CH_4	H_2O	1608.0	−2.059	499.2	−0.2550
C_2H_4	H_2O	1354.0	−1.542	346.5	−0.3326
C_2H_6	H_2O	1529.0	−3.081	405.0	0.0930

Table 4
Deviations between experimental data and predicted results of the Model

System	T (K)	P (bar)	Number of data points (N)	$(\Delta \ln K)_{aver}$[a]	Ref.
H_2–H_2O	311–589	3–138	13	0.05	[28]
H_2–CO–H_2O	3–138	311–589	15	0.07	[28]
CH_4–H_2O	323–589	14–169	16	0.06	[29]
CO_2–H_2O	302–477	7–202	8	0.04	[29]

[a] $(\Delta \ln K)_{aver} = \sum_{i=1}^{N}\sum_{j=1}^{C}|\ln K_{j,cal} - \ln K_{j,exp}/CN|$, where K_j is equilibrium ratios of component j, C is number of components.

$\partial(n\alpha)/\partial n_i$ can be calculated from the MHV2 mixing rule (Eq. (10)), using:

$$(q_1 + 2\alpha q_2)\frac{\partial(n\alpha)}{\partial n_i} = q_1\alpha_{ii} + q_2(\alpha^2 + \alpha_{ii}^2) + \ln\gamma_i + \ln\frac{b}{b_{ii}} + \frac{b_{ii}}{b} - 1 \quad (21)$$

Table 4 shows deviation between model predicted and experimental data [28,29]. In all cases the average deviation of the logarithm of the equilibrium ratios is small, i.e. predicted values are in agreement with experimental results.

3.3. Enthalpy and entropy of real fluid and biomass

The enthalpy of real gas is represented by

$$H = H^* + H^R \quad (22)$$

The first term on the right-hand side of Eq. (22) is the enthalpy of ideal gas

$$H^* = H_o^* + \int_{T_0}^{T} C_p^* \, dT \quad (23)$$

where H_o^* is enthalpy at reference state, and C_p^* is specific heat capacity of ideal gas which is a function of temperature. Table 5 displays the enthalpy and entropy at the reference state, and heat capacity of ideal gases.

The second term on the right-hand side of Eq. (22) is residual enthalpy, which is expressed as

$$H^R = \int_{\infty}^{V}\left[T\left(\frac{\partial P}{\partial T}\right)_V - P\right] dV + RT(Z-1) \quad (24)$$

where V is the specific volume of real gas and is calculated by state equation of SRK (Eq. (5)).

Reaction equation of biomass combustion is

$$CH_xO_y(s) + \left(1 + \frac{x}{4} - \frac{y}{2}\right)O_2(g) \rightarrow CO_2(g) + \frac{x}{2}H_2O(g) \quad (25)$$

And the lower heating value of biomass is given by

$$LHV_{biomass} \approx \sum -V_i H_{i[298.15\ K,1\ atm]} \quad (26)$$

from which the enthalpy of real biomass at reference state can be calculated.

The entropy of real gas is represented by

$$S = S^* + S^R \quad (27)$$

S^* is the entropy of ideal gas

$$S^* = S_o^* + \int_{T_0}^{T}\frac{C_p^*}{T}\, dT - R\ln\frac{P}{P_o} \quad (28)$$

where S_o^* is entropy at reference state. Residual entropy is given by

$$S^R = \int_{\infty}^{V}\left[\left(\frac{\partial P}{\partial T}\right)_V - \frac{R}{V}\right] dV + R\ln\frac{V}{V_o} \quad (29)$$

The enthalpy and entropy of water are calculated by a modified formula based on the data formulation IAPWS 1995 [30]

$$H = H_o^* + [\bar{H}(T, P) - \bar{H}\ (298.15\ K, 1\ atm)] \quad (30)$$

$$S = S_o^* + [\bar{S}(T, P) - \bar{S}\ (298.15\ K, 1\ atm)] \quad (31)$$

where H_o^* and S_o^* are the enthalpy and entropy of water at reference state, respectively, $\bar{H}(T, P)$ and $\bar{S}(T, P)$ are the enthalpy and entropy of water at T, P given by the data formulation IAPWS 1995, respectively.

3.4. Exergy of real fluid and biomass

Exergy of a material stream includes chemical exergy ($E_{X,c}$) and physical exergy ($E_{X,ph}$), and total exergy of a material stream is given as

$$E_X = E_{X,c} + E_{X,ph} \quad (32)$$

Table 5
Enthalpy and entropy at the reference state, and heat capacity of an ideal gas

	$C_p^* = A + BT + BT^2 + BT^3$ (J/(mol K))				H_o^* (kJ/mol)	S_o^* (J/(mol K))
	A	$B \times 10^2$	$C \times 10^5$	$D \times 10^8$		
H_2	29.062	−0.82	0.199	0.0	0.0	130.59
O_2	25.594	13.251	−0.421	0.0	0.0	205.03
CO	26.537	7.683	−0.1172	0.0	−110.52	197.91
CO_2	26.748	42.258	−1.425	0.0	−393.51	213.64
CH_4	25.36	1.687	7.131	−4.084	−74.85	186.19
C_2H_4	3.798	15.65	−8.346	1.756	52.28	219.45
C_2H_6	8.181	16.147	−4.007	−0.694	−84.67	229.49
H_2O(l)					−285.84	69.94

Physical exergy is resulted from the difference in temperature and pressure between operation condition and reference environmental condition. The physical exergy of a pure compound in a mixture can be easily calculated using enthalpy and entropy data for the given system:

$$E_{X,ph} = (H - H_o) - T_0(S - S_o) \tag{33}$$

where H and S are enthalpy and entropy of a system at given temperature and pressure, and H_o and S_o are the values of these functions at the environmental temperature and pressure. Value of the physical exergy of biomass is assumed to be zero in this paper.

The physical exergy of gas mixture is derived from the conventional linear mixing rule

$$E_{X,ph} = \sum_i y_i E^i_{X,ph} \tag{34}$$

and the chemical exergy of gas mixture is given by

$$E_{X,c} = \sum_i y_i \varepsilon_{0,i} + RT_0 \sum_i y_i \ \ln y_i \tag{35}$$

where $\varepsilon_{0,i}$ is the standard chemical exergy of a pure chemical compound i. $\varepsilon_{0,i}$ is equal to the maximum amount of work obtainable when a compound is brought from the environmental state, characterized by the environmental temperature T_0 and environmental pressure P_0, to the dead state, characterized by the same environmental conditions of temperature and pressure, but also by the concentration of reference substances in standard environment. A standard environment model given by Szargut was used in this paper.

The chemical exergy of biomass is hard to define and therefore, the statistical correlation of Szargut and Styrylska was used [31]:

$$\varepsilon_{0,biomass} = \beta \mathrm{LHV}_{biomass} \tag{36}$$

where $\mathrm{LHV}_{biomass}$ is the lower heating value, and

$$\beta = \frac{1.0412 + 0.2160(Z_H/Z_C) - 0.2499 Z_O/Z_C[1 + 0.7884 Z_H/Z_C] + 0.0450 Z_N/Z_C}{1 - 0.3035 Z_O/Z_C} \tag{37}$$

Z_O, Z_C, Z_H and Z_N are the weight fractions of oxygen, carbon, hydrogen and nitrogen, respectively, in the biomass.

Heating is needed in the biomass gasification system, and the thermal exergy is

$$E_{X,Q} = \int \left(1 - \frac{T_0}{T}\right) \delta Q \tag{38}$$

3.5. Energy and exergy efficiencies

The equation of energy conservation for stable material stream is given by

$$\dot{Q} = \dot{W} + \Delta \dot{H} \tag{39}$$

The equation of exergy balance is

$$\sum_{in} E_i = \sum_{out} E_k + I \tag{40}$$

where $\sum_{in} E_i$ and $\sum_{out} E_k$ are the exergy flow of all input and output material streams, respectively. I is the internal exergy loss due to irreversibility.

Energy efficiency and energy loss ratio are defined, respectively, as

$$\eta_{en} = \frac{E_{n,out}}{E_{n,in}} \times 100\% \tag{41}$$

and

$$\sigma_{en} = \frac{(E_{n,loss})_i}{\sum (E_{n,loss})_i} = \frac{(E_{n,loss})_i}{E_{n,loss}} \times 100\% \tag{42}$$

Similarly, exergy efficiency and exergy loss ratio are defined, respectively, as

$$\eta_{ex} = \frac{E_{x,out}}{E_{x,in}} \times 100\% \tag{43}$$

and

$$\sigma_{ex} = \frac{(E_{x,loss})_i}{\sum (E_{x,loss})_i} = \frac{(E_{x,loss})_i}{E_{x,loss}} \times 100\% \tag{44}$$

4. Results and discussion

4.1. Chemical equilibrium in the reactor

When the calculation is conducted, H_2, CH_4, CO_2, CO, C_2H_4, C_2H_6, H_2O and solid carbon are considered in the chemical equilibrium model. Wood sawdust, which is represented by a general formula of $CH_{1.35}O_{0.617}$, is used as a typical gasification material in this paper. The predicted results show that the yields of C_2H_4, C_2H_6 and solid carbon are less than 10^{-5} mol/kg dry biomass, much less than other species, so these two species can be neglected and the product gas were considered to include mainly H_2, CH_4, CO and CO_2.

4.1.1. Effects of temperature on chemical equilibrium

Fig. 2 shows the variation of equilibrium gas yields at with temperature ranging from 673 K to 1073 K. The yields of H_2 and CO_2 increase with the increasing temperature, while the yield of CH_4 decreases sharply. Therefore, higher temperature favors H_2 production. CO yield is very small, about 10^{-3} mol/kg dry biomass. As temperature increases from 673 K to 1073 K, the CO yield increases first and then decreases. CO yield reaches maximum at about 823 K. Note that H_2 yield increases very slowly at high temperature and become nearly unchanged since about 923 K, and then gas product contains almost only H_2 and CO_2. The maximal H_2 yield of 88.623 mol/kg dry biomass is obtained. Consequently, from the viewpoint of thermodynamics, further increase of temperature is unnecessary for H_2 production.

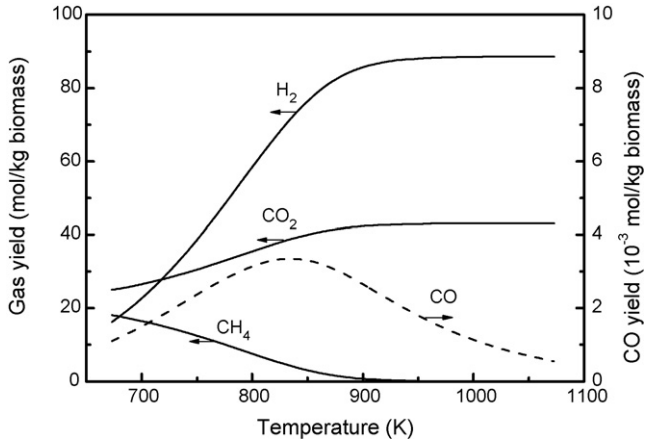

Fig. 2. Equilibrium gas yields in the reactor as a function of temperature for biomass gasification at 25 MPa with 5 wt% dry biomass content.

4.1.2. Effects of feedstock concentration on chemical equilibrium

Fig. 3 displays the effects of feedstock concentration in the reactor on equilibrium gas yield at 873 K and 25 MPa. As shown in Fig. 3, H_2 and CO_2 yields decrease gradually with increasing feedstock concentration, while CH_4 and CO yields increase. The product gas consists of mainly H_2 and CO_2 when biomass feedstock concentration is low, but the CH_4 yield becomes remarkable when the feedstock concentration is high. The objective of biomass gasification in SCW is to produce H_2, so it is better for the system to operate with high biomass feedstock concentration and produce as little CH_4 as possible. Since CH_4 yield decreases with increasing temperature, as mentioned above, high reaction temperature seems necessary to achieve high H_2 yield with high feedstock concentration. To realize the effective gasification of biomass with high feedstock concentration at lower temperature, a special layout of the experimental system was proposed. As shown in Fig. 1, high concentration biomass feedstock mixes with high temperature water at the inlet of reactor and gets diluted, while water and heat were recycled. With this layout, biomass is fed to the system at high concentration, while gasified in the reactor at low concentration. For example,

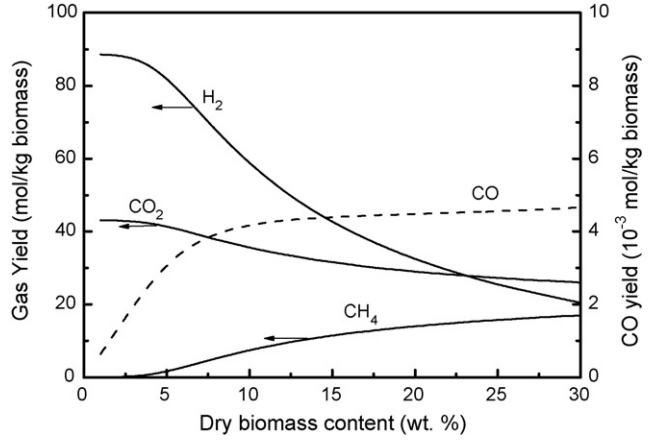

Fig. 3. Equilibrium gas yields in the reactor as a function of dry biomass content for biomass gasification at 25 MPa, 873 K.

biomass is fed with the flowrate of 2 kg/h and the concentration of 30 wt%, and the flow rate of high temperature water is 10 kg/h, the concentration of biomass in reactor is actually 5 wt%. As a result, the biomass feedstock at high concentration can be gasified at lower temperature.

4.1.3. Effects of oxygen addition on chemical equilibrium

Biomass gasification in SCW is an endothermic reaction, so the process requires extra heat to drive the chemical reaction. Generally, heat is supplied to the reactor from external heat resource, but exergy and energy loss will be caused due to heat transfer. Also, fast heating and complete gasification of biomass are difficult to achieve with external heating. Considering that biomass can be oxidized to be CO_2 and H_2O by oxygen in SCW and generate heat, oxygen can be added to the reactor to realize internal heat supply for the biomass gasification reaction. High heat transfer efficiency and gasification efficiency are also gained.

Some experimental studies on partial oxidation of biomass in SCW for hydrogen production have been conducted recently [32,33]. Here, the effects of oxygen addition on the equilibrium gas yield are investigated by thermodynamic calculation. Equivalence ratio (ER) represents the amount of oxygen addition, and is defined as

$$\mathrm{ER} = \frac{\text{weight oxygen/weight dry biomass}}{\text{stoichiometric/biomass ratio}} \tag{45}$$

Fig. 4 shows the effects of oxygen addition on equilibrium gas yield at 25 MPa with various temperatures. It can be seen that H_2 and CH_4 yields decrease with the increasing amounts of oxygen addition under the same temperature and pressure. Fig. 5 displays the variation of external energy requirement in the gasification reactor with oxygen ER for equilibrium state at 873 K, 25 MPa. The external energy requirement decreases with increasing oxygen ER. But even when ER is to 0.5, which means only a half of H_2 yield can be obtained compared with that of no oxygen addition, the external energy requirement is still greater than 1000 W. As a result, to realize full self-heating, larger ER value is needed and leads to even less hydrogen production. In fact, most heat generated from biomass oxidation was absorbed by the water but not used effectively for the reaction. In the system proposed by Hong et al. [32], auxiliary fuel, such as waste ethanol, is added to heat the reactor internally by its oxidation reaction and high hydrogen yield is obtained.

4.2. Gas–liquid phase equilibrium in high-pressure separator

It is assumed that chemical equilibrium is reached when biomass feedstock with concentration of 5 wt% is gasified in the reactor at 873 K, 25 MPa, and then reaction products enter the high-pressure separator.

4.2.1. Effects of pressure on gas–liquid equilibrium

Fig. 6 displays the effects of pressure in SPE1 on hydrogen recovery ratio (defined as the amount of hydrogen in gas phase of SPE1/total amount of hydrogen in the product gas), gas com-

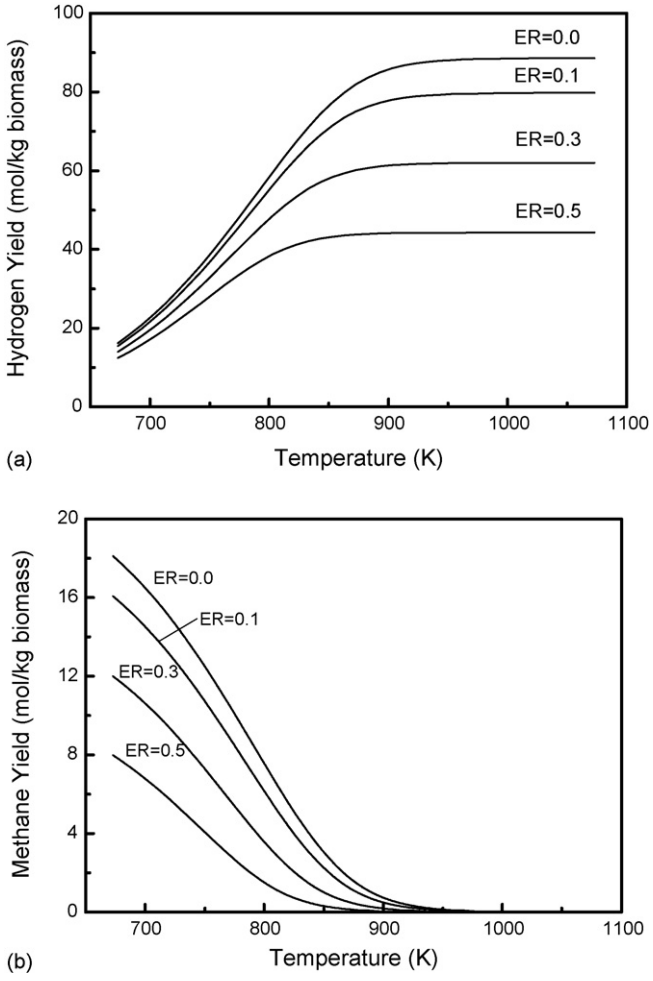

Fig. 4. The equilibrium hydrogen yield (a), methane yield (b) as a function of reaction temperature with different oxygen equivalence ratio. The dry biomass content in the reactor is 5 wt% and the reaction pressure is 25 MPa.

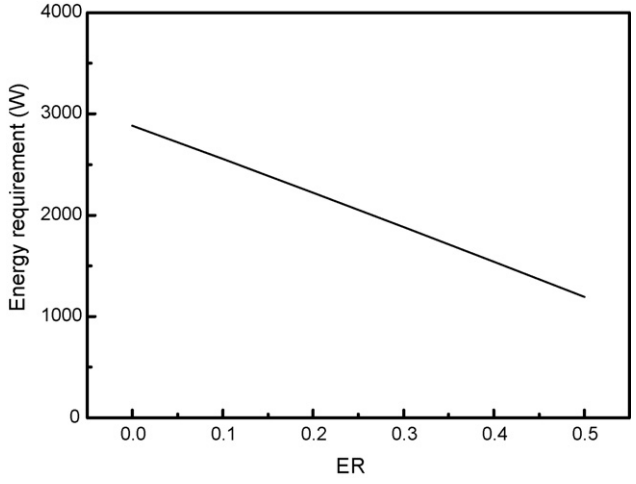

Fig. 5. The external energy requirement in the gasification reactor as a function of oxygen equivalence ratio. It is assumed that the temperature and pressure of biomass gasification system are 873 K and 25 MPa, respectively. The mass flow rate of biomass feedstock (pump 1 in Fig. 1) is 2.0 kg/h at 298 K and feedstock concentration is 30 wt%. The mass flow rate of the pure water stream (pump 2 in Fig. 1) inputting the reactor is 10 kg/h and the temperature is 873 K.

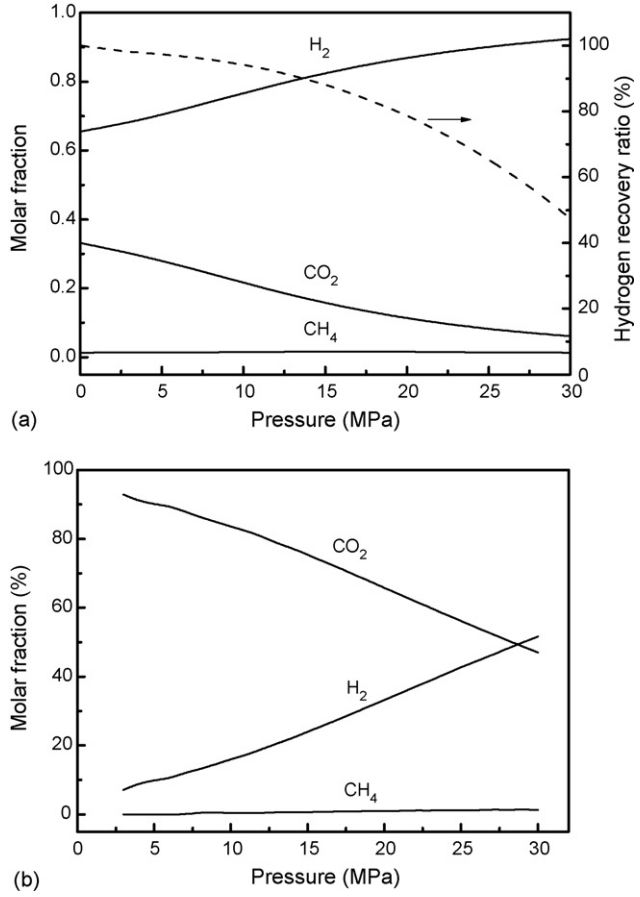

Fig. 6. Effects of operation pressure in SPE1 on separating H_2 from CO_2 at 298 K: (a) gas composition and hydrogen recovery ratio in gas phase in SPE1, (b) gas composition in liquid phase in SPE1.

position in gas phase and liquid phase in SPE1 at 298 K. It is shown in Fig. 6(a) that the molar fraction of hydrogen in the gas phase increases from 65.56% to 92.41% and the molar fraction of CO_2 decreases sharply from 33.11% to 6.12% with the pressure in SPE1 increasing from 0.1 MPa to 30 MPa. The Henry constants of CO and CH_4 are all greater than that of H_2, so most of CO and CH_4 leave the high-pressure separator with the gas phase stream and contaminate the H_2. It is can be also seen that hydrogen recovery ratio decreases and the molar fraction of CH_4 has a little tendency to increase with the increasing pressure.

Fig. 6(b) shows that the molar fraction of CO_2 in the liquid phase decreases and the molar fraction of H_2 increases with the pressure in SPE1. Combination of Fig. 6(a and b) suggests that increasing the pressure in SPE1 favors the purity of H_2 in the gas phase but decreases the hydrogen recovery ratio, so appropriate operation pressure of SPE1 must be selected. The predicted results show that H_2 of 82.45% and recovery ratio of 88.15% are obtained at 15 MPa, 298 K.

4.2.2. *Effects of temperature on gas–liquid equilibrium*

Fig. 7 displays the effects of the SPE1 operation temperature on the high-pressure separation process with the SPE1operation pressure of 15 MPa. As shown in Fig. 7(a), as operation temperature increases, the molar fraction of H_2 in gas phase decreases

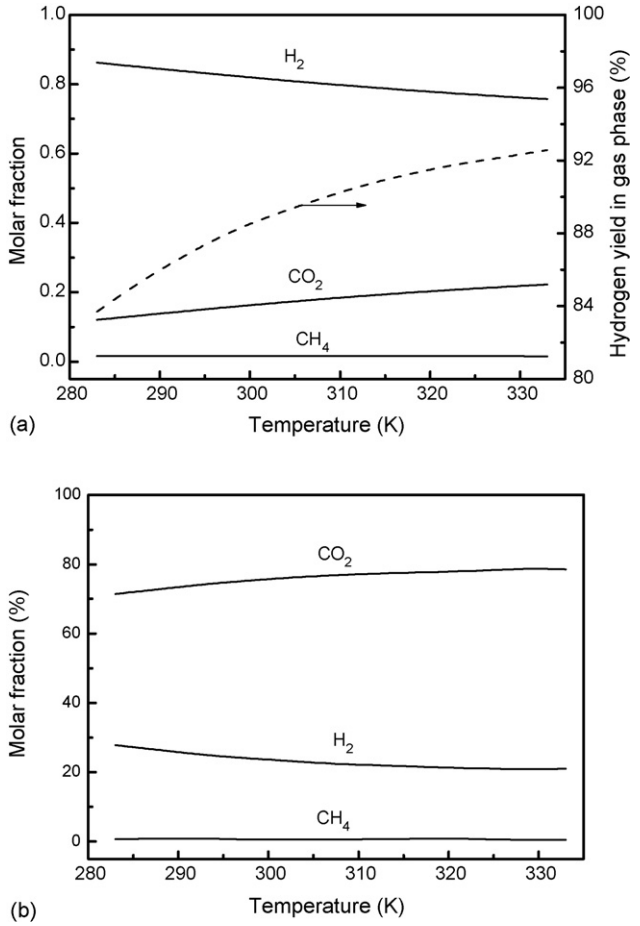

Fig. 7. Effects of operation temperature in SPE1 on separating H_2 from CO_2: (a) gas composition and hydrogen recovery ratio in gas phase in SPE1, (b) gas composition in liquid phase in SPE1.

while the molar fraction of CH_4 and CO_2 increase, and the hydrogen recovery ratio also increases. Purity of H_2in the gas phase is 86.24% at 283 K and 75.7% at 333 K, respectively. Fig. 7(b) shows the variation of gas composition in liquid phase with operation temperature. Note that the molar fraction of CO_2 increases and that of H_2 decreases with increasing temperature. As a result, proper operation temperature of SPE1 should be selected to consider both H_2 purity and hydrogen recovery ratio. H_2 and CH_4 in the liquid phase can be separated in SPE2 and combust with oxygen to produce heat, which can be recycled for the gasification system to reduce external heat input.

4.2.3. Effect of water recycled ratio on gas–liquid equilibrium

The amount of CO_2 dissolved in water is limited, therefore, extra water need to be added into SPE1 when the amount of CO_2 is large. Water recycled ratio (defined as the mass flow rate of pump 3 in Fig. 1/the total mass flow rate of pump 1 and pump 2) is another important operation parameter of SPE1. Fig. 8 displays the effects of water recycled ratio on gas composition of SPE1 at 15 MPa, 298 K. It can be seen that the molar fraction of H_2 increases, the molar fraction of CO_2 decreases, while the hydrogen recovery ratio decreases sharply as water

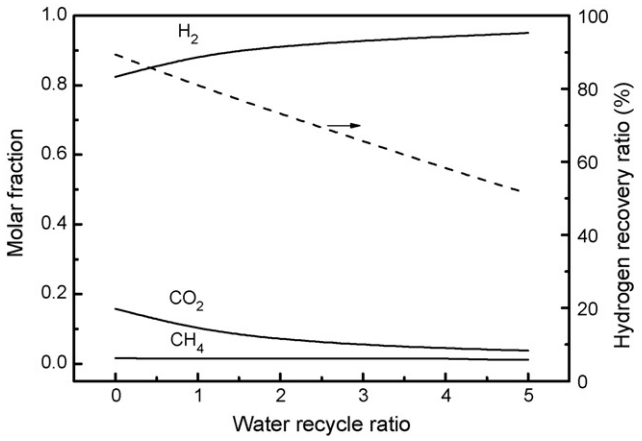

Fig. 8. Effects of water recycle ratio on gas composition and hydrogen recovery ratio in gas phase in SPE1. Operation pressure is 15 MPa and operation temperature is 298 K.

recycled ratio increases. Note that H_2 molar fraction increases more and more slowly because most CO_2 is dissolved in water when water recycled ratio is low. Since the amount of H_2 dissolved in water increases with increasing water recycled ratio, higher water recycled ratio leads to lower hydrogen recovery. Consequently, it is not necessary to add extra water into SPE1 when the gas and water ratio is small.

4.3. Energy and exergy analysis of the whole system

To conduct the energy and exergy analysis of the system, a set of typical operating parameters were chosen for the calculation. Operating temperature and pressure of the biomass gasification system are 873 K and 25 MPa, respectively. The mass flow rate of biomass feedstock (pump 1 in Fig. 1) is 2.0 kg/h, and feedstock concentration is 30 wt%. The mass flow rate of water stream (pump 2 in Fig. 1) is 10 kg/h and the temperature is 873 K. It is assumed that external heat resource is used to meet heat requirement of the system, that biomass gasification in the reactor reaches chemical equilibrium and that heat transfer efficiency of the reactor equals to that of the preheater.

4.3.1. Energy and exergy losses of the system

Table 6 displays the results of energy and exergy analysis of the biomass gasification system. It is shown that energy efficiency of the system is 44.21% and the exergy efficiency is 42.26% under the calculation conditions. Energy loss is caused mainly by heat transfer and the loss from heat exchanger, cooler, preheater and reactor takes up 94.67% of the total. Energy loss from heat exchanger is the largest part and that from cooler is the second. Exergy loss represents the irreversibility of the system. Exergy loss of the biomass gasification system is caused mainly from reactor, heat exchanger and preheater. Exergy loss from these three units takes up 81.49% of the total, with that from reactor taking up 36.88%, heat exchanger 32.01% and preheater 12.6%. Exergy loss of the reactor is resulted from the irreversibility of both chemical reaction and heat transfer, while that of heat exchanger and preheater is only from heat transfer irreversibility. Therefore, heat transfer efficiency of the biomass gasification

Table 6
Exergy and energy analysis of hydrogen production by biomass gasification in SCW

	$E_{x,loss}$ (W)	σ_{ex} (%)	$E_{n,loss}$ (W)	σ_{en} (%)
Pump 1[a]	22.62	0.44	23.40	0.43
Reactor[b]	1882.84	36.88	971.01	17.90
Heater exchanger[c]	1634.21	32.01	2581.77	47.61
Preheater	643.18	12.60	534.66	9.86
Pump 2	161.56	3.16	177.12	3.27
Cooler	100.71	1.97	1046.59	19.30
Valve 1	83.31	1.63	26.76	0.49
Valve 2	97.25	1.90	0.44	0.01
SEP1 + SEP2[d]	187.65	3.68	23.75	0.44
PSA[e]	292.23	5.72	37.69	0.69
Σ	5105.56	100	5423.19	100
η_{ex} (%)	42.46			
η_{en} (%)	44.21			

[a] The energy efficiency of all high pumps is 30%, the temperature of the initial biomass feedstock is 298 K, and LHV of biomass is 18425.97 kJ/kg.
[b] The heat resource temperature of reactor and preheater is 1273 K, and the heat transfer efficiency is 75%.
[c] The heat transfer efficiency is 75%, and the high temperature fluid is cooled to the temperature of 373 K.
[d] The operation temperature and pressure are 298 K and 15 MPa, respectively. The water recycled ratio is 0, and the gas compositions of gas phase and liquid phase in high-pressure separator are calculated by gas–liquid equilibrium model.
[e] The feed pressure of PSA is 4 MPa, the tail gas pressure is 0.1 MPa, and the hydrogen recovery ratio is 90%. The energy requirement of PSA is 4.46 kWh/kmol CO_2.

system is the key to the improvement of total energy and exergy efficiencies. Effects of heat transfer efficiency of reactor, heat exchanger and preheater were analyzed as follows.

4.3.2. *Effects of heat transfer efficiency on total energy and exergy efficiencies*

Fig. 9 shows the effects of heat transfer efficiency in heat exchanger on the total energy and exergy efficiencies. As expected, total energy and energy efficiencies of the biomass gasification increase with the increase of heat transfer efficiency in the heat exchanger. The increasing tendency is even more obvious with higher heat transfer efficiency in the heat exchanger. Fig. 10 displays the effects of heat transfer efficiency in reactor and preheater. It can be seen that increase of heat transfer efficiency in reactor and preheater can also results in the increase of total energy and energy efficiencies.

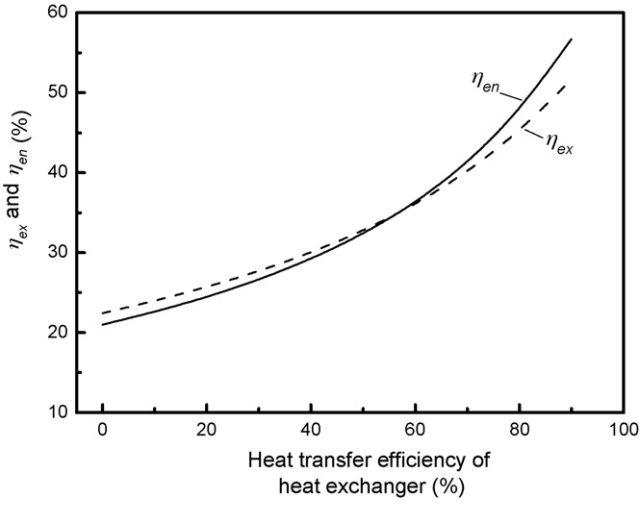

Fig. 9. Effects of heat transfer efficiency of heat exchanger on the energy conversion efficiency of gasification system. The heat transfer efficiency of reactor and preheater is 75%, and the temperature of external heat resource is 1273 K.

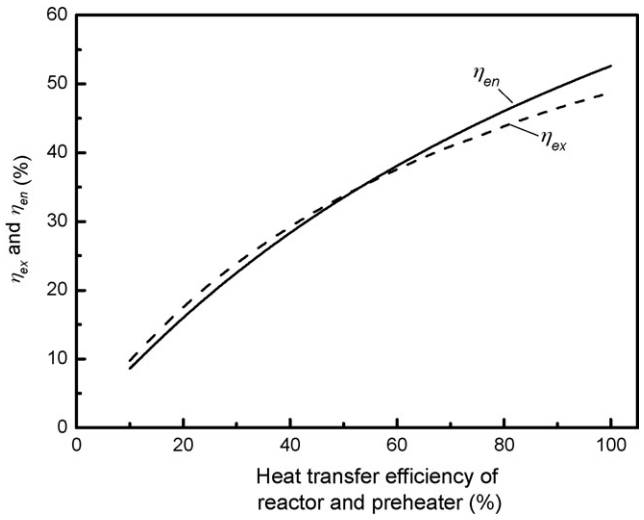

Fig. 10. Effects of heat transfer efficiency of reactor and preheater on the energy conversion efficiency of gasification system. The heat transfer efficiency of heat exchanger is 75%, and the temperature of external heat resource is 1273 K.

4.3.3. *Effects of heat resource on total energy and exergy efficiencies*

Table 7 shows the effect of the temperature of external heat resource on total energy and exergy efficiency. As is shown in the table, total energy efficiency keeps unchanged with the variation of the temperature of external heat resource, because energy input and output of the system does not change. However, heat at high temperature includes more exergy than that at low temperature, so the exergy efficiency decreases with increasing temperature of external heat resource. Solar thermal energy can be considered to be a heat resource with the temperature of 5800 K. Total exergy efficiency of the gasification system can be up to 37.8% if solar energy is used as the external heat source. Solar energy is abundant and clean, therefore, solar energy can be used as a potential external heat source for the biomass thermo-chemical gasification process. Coupling of hydrogen production from biomass gasification in SCW and solar energy heating will achieve a renewable energy conversion process indeed.

Table 7
Comparison of energy and exergy efficiency with different heating methods[a]

	Temperature of heat resource (K)			
	1073	1273	1473	5800 (solar thermal)
η_{en} (%)	44.21	44.21	44.21	44.21
η_{ex} (%)	43.75	42.26	41.57	37.80

[a] The heat transfer efficiency of the reactor, preheater and heat exchanger is 75%.

5. Conclusion

The thermodynamic models proposed in this paper can be used to predict product gas composition at chemical equilibrium for the gasification in SCW, to assess the H_2 purification at the phase equilibrium in the high-pressure separator, and to calculate the energy and exergy efficiencies of the whole system. The models are able to provide information for design, development and optimization of H_2 production using biomass gasification in SCW. The results from chemical equilibrium analysis show that high temperature is in favor of hydrogen production. When biomass is gasified with addition of less than stoichiometric quantities of oxygen, the reactor can get its heat from the in situ exothermic oxidation reaction but H_2 and CH_4 yields decrease with the increasing amounts of oxygen addition. Results from phase equilibrium of the high-pressure separator show that the increasing pressure and temperature favors the purity of hydrogen in the gas phase but decreases the hydrogen recovery ratio, so appropriate operation pressure and temperature must be selected. Results of energy and exergy analysis of the gasification system show that energy and exergy efficiency of the whole system can be more than 40%. The energy loss is mainly from heat exchanger, cooler, preheater and reactor, and the exergy loss is from the reactor, heat exchanger and preheater, which are mostly resulted from heat transfer in the system. Consequently, high heat transfer efficiency will result in high energy and exergy efficiency of the whole system.

Acknowledgements

This work is currently supported by the National Key Project for Basic Research of China through contract No. 2003CB214500 and the National Natural Science Foundation of China through contract No. 50521604.

References

[1] A. Kruse, A. Gawlik, Biomass conversion in water at 330–410 °C and 30–50 MPa: identification of key compounds for indication different chemical reaction pathways, Ind. Eng. Chem. Res. 42 (2) (2003) 267–279.

[2] P.E. Savage, Organic chemical reactions in supercritical water, Chem. Rev. 99 (1999) 603–621.

[3] P.T. Williams, J. Onwudili, Composition of products from the supercritical water gasification of glucose: a model biomass compound, Ind. Eng. Chem. Res. 44 (2005) 8739–8749.

[4] D.C. Elliott, L.J. Sealock, E.G. Baker, Chemical processing in high-pressure aqueous environments. 2. Development of catalyst of gasification, Ind. Eng. Chem. Res. 32 (1993) 1542–1548.

[5] D.C. Elliott, L.J. Sealock, E.G. Baker, Chemical processing in high-pressure aqueous environments. 3. Batch reactor process development experiments for organics destruction, Ind. Eng. Chem. Res. 33 (1994) 558–565.

[6] D. Yu, M. Aihara, J.M. Antal, Hydrogen production by steam reforming glucose in supercritical water, Energy Fuel 7 (1993) 574–577.

[7] J.M. Antal, S.G. Allen, D. Schulman, X. Xu, R.J. Divilio, Biomass gasification in supercritical water, Ind. Eng. Chem. Res. 39 (2000) 4044–4053.

[8] T. Minowa, F. Zhen, T. Ogi, Cellulose decomposition in hot-compressed water with alkali or nickel catalyst, J. Supercrit. Fluids 13 (1998) 253–259.

[9] T. Yoshida, Y. Matsumura, Gasification of cellulose, xylan and lignin mixtures in supercritical water, Ind. Eng. Chem. Res. 40 (2001) 5469–5474.

[10] T. Yoshida, Y. Oshima, Y. Matsumura, Gasification of biomass model compounds and real biomass in supercritical water, Biomass Bioenergy 26 (2004) 71–78.

[11] H. Schmieder, J. Abeln, N. Boukis, E. Dinjus, A. Kruse, M. Kluth, G. Petrich, E. Sadri, M. Schacht, Hydrothermal gasification of biomass and organic wastes, J. Supercrit. Fluids 17 (2000) 145–153.

[12] A. Kruse, T. Henningsen, A. Sinag, J. Pfeiffer, Biomass gasification in supercritical water: influence of the dry matter content and the formation of phenols, Ind. Eng. Chem. Res. 42 (2003) 3711–3717.

[13] A. Sinag, A. Kruse, J. Rathert, Influence of the heating rate and type of catalyst on the formation of key intermediates and on the generation of gases during hydropyrolysis of glucose in supercritical water in a batch reactor, Ind. Eng. Chem. Res. 43 (2004) 502–508.

[14] X.H. Hao, L.J. Guo, X. Mao, X.M. Zhang, X.J. Chen, Hydrogen production from glucose used as a model compound of biomass gasified in supercritical water, J. Int. Hydrogen Energy 28 (2003) 55–64.

[15] X.H. Hao, L.J. Guo, X.M. Zhang, Y. Guan, Hydrogen production from catalytic gasification of cellulose in supercritical water, Chem. Eng. J. 110 (2005) 57–65.

[16] Y.J. Lu, L.J. Guo, C.M. Ji, X.M. Zhang, X.H. Hao, Q.H. Yan, Hydrogen production by biomass gasification in supercritical water: a parametric study, J. Int. Hydrogen Energy 31 (2006) 822–831.

[17] H. Tang, K. Kitagawa, Supercritical water gasification of biomass: thermodynamic analysis with direct Gibbs free energy minimization, Chem. Eng. J. 106 (2005) 261–267.

[18] Q.H. Yan, L.J. Guo, Y.J. Lu, Thermodynamic analysis of hydrogen production from biomass gasification in supercritical water, Energy Convers. Manage. 47 (2006) 1515–1528.

[19] W. Feng, H.J. Kooi, A.J. Swaan, Biomass conversions in subcritical and supercritical water: driving force, phase equilibria, and thermodynamic analysis, Chem. Eng. Process. 43 (2004) 1459–1467.

[20] Y. Calzavara, C. Joussot-Dubien, G. Boissonnet, S. Sarrade, Evaluation of biomass gasification in supercritical water process for hydrogen production, Energy Convers. Manage. 46 (2005) 615–631.

[21] Y. Matsumura, T. Minowa, Fundamental design of a continuous biomass gasification process using a supercritical water fluidized bed, J. Int. Hydrogen Energy 29 (2004) 701–707.

[22] Y. Yoshida, K. Dowaki, Y. Matsumura, R. Matsuhashi, D. Li, H. Ishitani, H. Komiyama, Comprehensive comparison of efficiency and CO_2 emissions between biomass energy conversion technologies—position of supercritical water gasification in biomass technologies, Biomass Bioenergy 25 (2003) 257–272.

[23] Z.H. Duan, N. Moller, J.H. Weare, A general equation of state for supercritical fluid mixture and molecular dynamics simulation of mixture PVTX properties, Geochim. Cosmochim. Acta 60 (1996) 1029–1216.

[24] P.M. Mathias, T.W. Copeman, Extension of the Peng–Robinson equation of state to complex mixture: evaluation of the various forms of the local composition concept, Fluid Phase Equilib. 13 (1983) 91–108.

[25] S. Dahl, M.L. Michelsen, High-pressure vapor–liquid equilibrium with a UMFAC-based equation of state, AIChE J. 36 (1990) 1829–1836.

[26] B.L. Larsen, P. Rasmussen, A. Fredenslund, A modified UNIFAC group-contribution model for prediction of phase equilibria and heats and mixing, Ind. Eng. Chem. Res. 26 (1987) 2274–2286.

[27] S. Dahl, A. Fredenslund, P. Rasmussen, The MHV2 model: a UNIFAC-based equation of state model for prediction of gas solubility and vapor-liquid equilibria at low and high pressure, Ind. Eng. Chem. Res. 30 (1991) 1936–1945.

[28] W. Wagner, A. Pruß, The IAPWS formulation 1995 for the thermodynamic properties of ordinary water substance for general and scientific use, J. Phys. Chem. Ref. Data 31 (2002) 387–535.

[29] P.C. Gillespie, G.M. Wilson, Vapor–liquid equilibrium data on water substitute gas components: N_2–H_2O, H_2–H_2O, CO–H_2O, H_2–CO–H_2O and H_2S–H_2O, Gas Processors Association Research Report No. 41, Wilco Research Co., Provo, UT, April 1980.

[30] P.C. Gillespie, G.M. Wilson, Vapor–liquid equilibrium and liquid–liquid equilibrium: H_2O–CH_4, H_2O–CO_2, H_2O–H_2S, H_2O–pentane, Gas Processors Association Research Report No. 48, Wilco Research Co., Provo, UT, April 1982.

[31] M.J. Prins, K.J. Ptasinski, F.J.J.G. Janssen, Thermodynamics of gas-char reactions: first and second law analysis, Chem. Eng. Sci. 58 (2003) 1003–1011.

[32] G.T. Hong, M.H. Spritzer, Supercritical water partial oxidation, in: Proceedings of the 2002 U.S. DOE Hydrogen Program Review NREL/CP-610-32405, 2002.

[33] T. Yoshida, Partial oxidative and catalytic biomass gasification in supercritical water: a promising flow reactor system, Ind. Eng. Chem. Res. 43 (2004) 4097–4104.